Magnetotunneling spectroscopy with the field perpendicular to the tunneling direction of the transverse X electrons in GaAs/AlAs double-barrier structures under hydrostatic pressure

J. M. Smith* and P. C. Klipstein
Clarendon Laboratory, Department of Physics, University of Oxford, Parks Road, Oxford OX1 3PU, United Kingdom

R. Grey and G. Hill
Department of Electrical and Electronic Engineering, University of Sheffield, Mappin Street, Sheffield S1 3JD, United Kingdom
(Received 9 March 1998)

We have measured the effect of in-plane magnetic field on tunneling resonances between transverse X states in GaAs/AlAs double-barrier structures under high hydrostatic pressure. Current-voltage and conductance-voltage measurements performed at pressures just beyond the type-II transition, and at fields up to 15 T, reveal clear field dependences of resonances originating from the $X_t(1) \rightarrow X_t(1)$ and $X_t(1) \rightarrow X_t(2)$ tunneling processes. Their behavior is consistent with a Lorenz force analysis, and therefore probes the in-plane electron dispersion around the X minima. Differences between measurements with the magnetic field oriented parallel to the [100] and [110] crystal axes reflect the anisotropy of the X minima, a first analysis indicating that the field dependence is dominated by the two X_t minima with large wave vectors perpendicular to the magnetic-field direction. In support of this, Schrödinger-Poisson modeling of the shift in bias position of the $X_t(1) \rightarrow X_t(2)$ resonance provides a value for the effective mass parallel to the Lorenz in-plane momentum vector which is consistent with the heavy principal effective mass of the X minima. [S0163-1829(98)01731-7]

I. INTRODUCTION

The conduction-band X minima of the AlAs electronic dispersion are of great interest, since the performance of GaAs/AlAs heterostructure devices such as resonant-tunneling diodes and superlattices is known to be affected significantly by their presence.[1–4] Increased access to the X minima is achieved by the application of hydrostatic pressure, which reduces their energy relative to the Γ minimum at a rate of about 13 meV kbar^{-1}. A type-I to type-II transition, in which the conduction-band ground state changes in nature from Γ_{GaAs} to X_{AlAs}, occurs at a pressure P_t ($\sim$9 kbar in wide layered structures), radically altering the optical and electrical properties of the system.

In double barrier structures (DBS's), strong current resonances between quasiconfined X states in the two AlAs layers may be observed at elevated pressures.[5–8] These are related to tunneling of electrons between transverse X (X_t) states,[7,8] since these states possess a lighter mass in the tunneling direction than do their longitudinal counterparts (X_l), and thus suffer much lower wave-function attenuation in the central GaAs layer. This is in contrast to single-barrier structures, in which transport via longitudinal states can dominate due to their increased coupling with the Γ_{GaAs} states in the contact region.[9] For AlAs thicknesses less than about 50 Å the lowest confined state in the AlAs is X_l, while for greater AlAs thicknesses it is X_t.[10] Therefore, AlAs layer thicknesses in excess of 50 Å are required in DBS's which exhibit strong high-pressure X-related resonances at 4.2 K.[8,10]

Magnetotunneling spectroscopy is a powerful tool for probing in-plane electronic dispersions of two-dimensional electron and hole gases, and has been performed on many systems in the past.[11–14] Here we report its application to tunneling between transverse X states in GaAs/AlAs heterostructures. In such DBS's with layer thicknesses greater than 50 Å, and with a suitable combination of hydrostatic pressure and applied electrical bias, the Fermi energy at low temperature is pinned very strongly to the emitter $X_t(1)$ state, creating a highly monoenergetic source of electrons for tunneling.[8] The semiclassical picture of the subsequent magnetotunneling of normally incident electrons, or a straightforward quantum-mechanical analysis, shows that for a magnetic field $(B_x,0,0)$,

$$\hbar \Delta k_y = -eB_x \Delta z. \tag{1}$$

Here Δk_y is the change of in-plane wave vector undergone by the tunneling electrons, and Δz is the distance traveled normal to the interfaces during the tunneling process. Orthogonal axes x and y are in the plane of the layers. To a first approximation, Δz is simply equal to the spatial separation of the well centers, d.

The requirement to conserve in-plane momentum in the tunneling process therefore translates into a change in resonant energetic alignment under the influence of B_x, given by

$$\Delta u = \frac{(eB_x d)^2}{2m_y^*}, \tag{2}$$

where u is defined as the energy difference between the $X_t(1)$ states in the two wells. By using a self-consistent Schrödinger-Poisson model described in Ref. 8, the shifts in bias position of observed current and conductance resonances can be converted into values of Δu, providing a means of calculating m_y^*.

 © 1998 The American Physical Society

II. EXPERIMENT

Four samples were studied in detail[8] which were nominally symmetric n-i-n GaAs/AlAs DBS's grown by molecular-beam epitaxy on [100]-oriented substrates. They were nominally identical with the exception of the AlAs layer thickness, which was varied in 10-Å increments between 40 and 70 Å. Labeling the AlAs layer width as l_w, the constituent epitaxial layers in the samples were as follows: 0.25-μm $n=1\times10^{18}$-cm^{-3} GaAs:Si buffer, 0.5-μm $n=2\times10^{17}$-cm^{-3} GaAs:Si, 100-Å undoped (ud) GaAs spacer, l_w-Å ud AlAs, 40-Å ud GaAs, l_w-Å ud AlAs, 100-Å ud GaAs spacer, 0.5-μm $n=2\times10^{17}$-cm^{-3} GaAs:Si and 0.25-μm $n=1\times10^{18}$-cm^{-3} GaAs:Si cap. Mesa diameters were 20 μm.

Of the four samples, the ones with 70- and 60-Å AlAs layers possess $X_t(1)$ ground states, and therefore display the most purely transverse characteristics at low temperatures that are most accurately analyzed by the Schrödinger-Poisson model of Ref. 8. The magnetotunneling characteristics of these two samples were similar in all respects.

The measurements presented here are for $l_w=70$ Å, and were taken at a temperature of 4.2 K and at pressures close to 9 kbar (each pressure measurement is accurate to within ±0.3 kbar), which is approximately 0.7 kbar beyond the type-II transition pressure P_t for this sample. The two terminal current-voltage measurements (I-V) were carried out using a combined voltage source and virtual ground current amplifier system, and conductance-voltage measurements (I'-V) were made by additionally modulating the dc applied voltage with a sinusoid of 1 mV rms, and $\sim$1 kHz, and subsequently detecting the ac component of the signal with a lock-in amplifier.

Orientation of the crystal to align its [100] and [110] axes parallel to the magnetic field was carried out manually and by eye, due to the constraints imposed by the pressure cell. The estimated tolerance on the stated orientations is therefore $\pm5°$. Additionally, measurements were performed with the longitudinal ([001]) orientation of the sample relative to the field, results of which will be used here to aid recognition of genuine in-plane field effects. A detailed report of this field orientation is presented elsewhere.[15]

III. RESULTS AND ANALYSIS

Magnetotunneling is most evident in the $X_t(1)\rightarrow X_t(1)$ resonance, since in the absence of **B** these states are energetically aligned at zero bias, and it is only due to the finite width of the allowed tunneling process that a current resonance is exhibited at a small bias either side of the origin. This width is predominantly a consequence of interface roughness and AlAs layer nonuniformity.[8]

The I'-V characteristics of the $X_t(1)\rightarrow X_t(1)$ resonance for all three field orientations are displayed in Fig. 1, in which strong peaks at zero bias clearly indicate the single resonant alignment in the absence of field. Slight differences between the zero-field curves are merely due to imperfect reproduction of applied pressure after sample reorientation.

For $\mathbf{B}\|[100]$ and $\mathbf{B}\|[110]$, the conductance peak splits clearly into two peaks at high field, with separations at 15 T of 50 and 65 mV, respectively, whereas with $\mathbf{B}\|[001]$ its

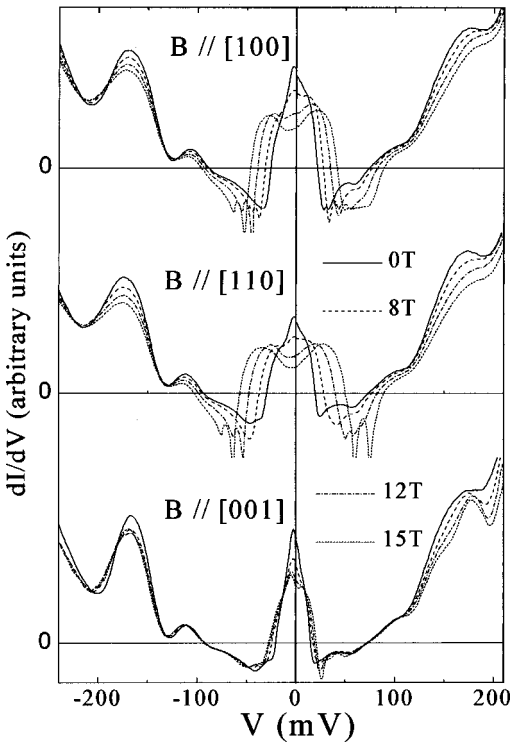

FIG. 1. Conductance curves for the sample with $l_w=70$ Å in three different **B** field orientations. With $\mathbf{B}\|[100]$ and $\mathbf{B}\|[110]$, a clear splitting of the $X_t(1)\rightarrow X_t(1)$ peak is observed, as a result of the in-plane wave vector supplied to the tunneling electrons [Eq. (1)]. $\mathbf{B}\|[001]$ (longitudinal orientation) is included for comparison. The pressures are approximately 9 kbar and the temperature is 4.2 K.

field dependence is minimal. The origin of the splitting, following from Eq. (2), is depicted in Fig. 2. It should be noted that, other than at zero bias, resonant alignment of states does not correspond exactly to the conductance peak, but it remains a good approximation for the low biases considered here. Figure 3 shows, correspondingly, an approximate doubling in the peak current density of the resonance under the influence of $\mathbf{B}\|[110]$.

An illustration of the physics behind the two in-plane orientations is given in Fig. 4. It can be seen that while a single Δu results from a given field in the [110] orientation, two very different values are expected for fields in the [100] orientation, corresponding to the different values of m_y^* for the pairs of X minima with their long wave vectors parallel with, and perpendicular to, B_x. These shall henceforth be labeled X_x and X_y, respectively. The data, however, display monotonic shifts in the conductance peak bias positions, and therefore indicate a single value of Δu, regardless of orientation. It therefore seems, at least for $\mathbf{B}\|[100]$, that one of these pairs of minima is dominant over the other. The fact that the bias splitting of the $X_t(1)\rightarrow X_t(1)$ resonance conduction peak is less for $\mathbf{B}\|[100]$ than for $\mathbf{B}\|[110]$ indicates that its Δu is correspondingly smaller, and so, from Eq. (2) and Fig. 4, also indicates that it is the X_y minima that dominate the tunneling current. It is, however, not possible to perform reliable quantitative analysis at this stage, since the present Schrödinger-Poisson model is likely to fail at such low biases because any uncertainty in the alignment of the emitter

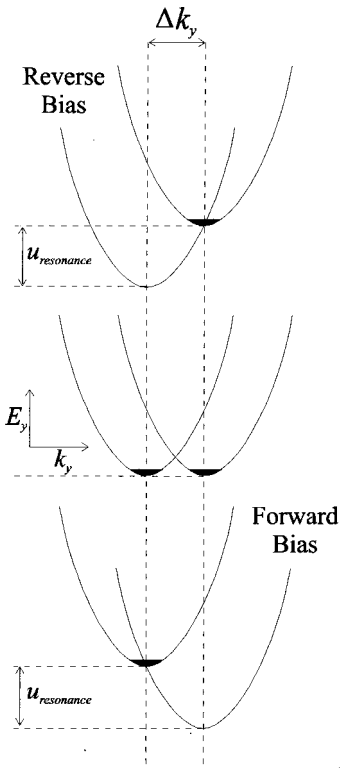

FIG. 2. Depiction of the splitting of the $X_t(1) \rightarrow X_t(1)$ conductance peak. The intersection of the in-plane dispersions of the emitter and collector X subbands represents the satisfaction of energy and momentum conservation conditions. Due to the in-plane momentum change Δk_y [Eq. (1)], and the highly monoenergetic population of the emitter state, two conductance peaks are resolved which correspond approximately to the forward and reverse bias occurrences of the interwell potential difference $u_{\text{resonance}}$.

and collector quasi-Fermi levels with their respective $X_t(1)$ states is comparable to the applied bias.

The interaction between an in-plane magnetic field and electrons in a square quantum well causes them to experience a potential additional to that formed by the band offsets,

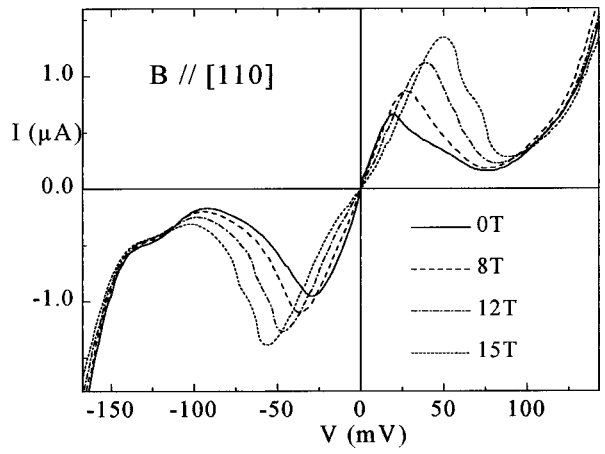

FIG. 3. I-V characteristics of the $X_t(1) \rightarrow X_t(1)$ resonance in a magnetic field $\mathbf{B} \| [110]$, under 9 kbar of hydrostatic pressure and at a temperature of 4.2 K. The weak features visible in the negative differential resistance region may not be genuine indications of resonant effects within the sample, since the measurement circuit may oscillate in this bias region.

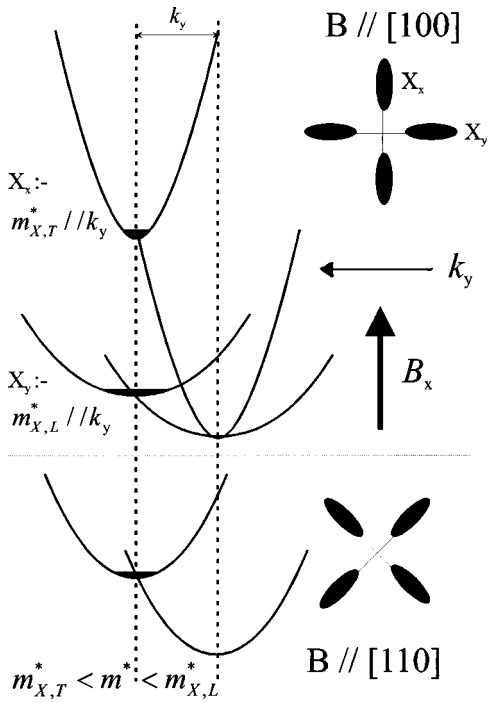

FIG. 4. A theoretical comparison between in-plane magnetotunneling in the [100] and [110] field orientations. In the former case, a stronger field dependence is expected from the resonant bias positions for the two X_x minima, than from those for the two X_y minima. The latter case is expected to show no such structure, since all four minima exhibit the same mass parallel to the induced wave-vector change. In the diagrams the two-dimensional layers are in the plane of the paper, and the electron flow is into the page.

which for small in-plane wave vectors is given approximately by[16,17]

$$\Delta V(B_x, B_y, z) = \frac{1}{2} \frac{e^2}{m_x^* m_y^*} (B_y^2 m_y^* + B_x^2 m_x^*)(z - z_0)^2, \tag{3}$$

where m_x^* and m_y^* are the principal effective masses in the yz plane, and z_0 is at the well center.

Keeping to our previous assignment of $B = B_x$, and considering $B \| [100]$, then m_y^* is much smaller for the X_x minima than it is for the X_y minima, and so the former experience a larger additional potential than do the latter. In this way the degeneracy of the X_x and X_y states is lifted, and X_y becomes the more heavily populated of the two. However, calculations of the expectation value of ΔV for the $X_t(1)$ emitter ground states show that at 15 T the $X_x - X_y$ splitting is only around 0.23 meV. This splitting is smaller than both the thermal energy at 4.2 K and the Fermi energy of the emitter $X_t(1)$ subband at zero bias, so it does not seem to explain adequately the complete lack of an X_x contribution that is apparent in our data. The only other plausible explanation is that the X_x contribution is lost within the negative differential resistance (NDR) of the X_y contribution (when the circuit oscillates, and the conductance data are not reliable) or within the phonon-assisted tunneling features at biases just beyond the NDR. This aspect will be the subject of further investigation.

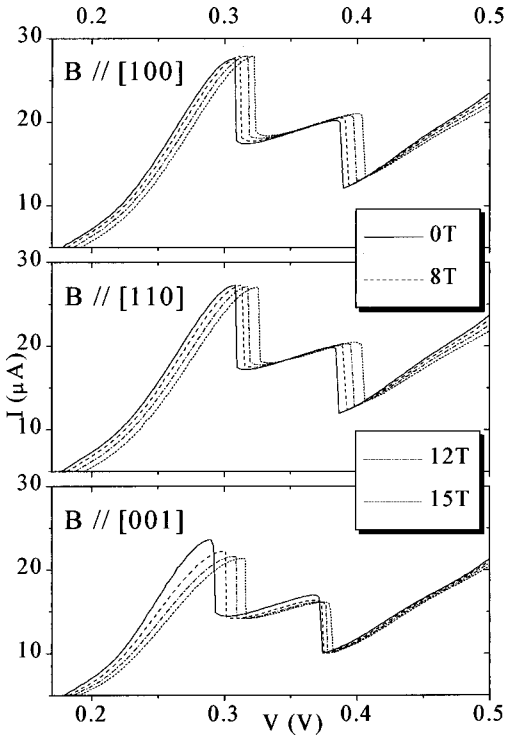

FIG. 5. Typical I-V plots showing the magnetic-field orientation dependence of the $X_t(1) \rightarrow X_t(2)$ resonance. With an in-plane field, a systematic increase in bias position is measured, consistent with the predictions of the Lorenz force theory. Furthermore, this increase is seen to be slightly greater for $\mathbf{B}\|[110]$ than for $\mathbf{B}\|[100]$, in support of the $X_t(1) \rightarrow X_t(1)$ data shown earlier. It is suspected that the [001] dependence is of a different origin than for the in-plane orientations, and may be related to the nonparabolicity of the X-band dispersion.

The $X_t(1) \rightarrow X_t(2)$ resonance shows a systematic increase in bias position with in-plane magnetic field. Comparison between typical I-V characteristics in each orientation are shown in Fig. 5. Despite the somewhat similar increase in peak bias position for the [001] orientation, it is thought that the *in-plane* field dependences of this resonance also derive from the increase in u given by Eq. (2). We note further that, again, the shift is larger for $\mathbf{B}\|[110]$ than for $\mathbf{B}\|[100]$, and that again there is no visible separation into X_x and X_y components for $\mathbf{B}\|[100]$. For the [001] orientation the peak current decreases significantly with bias, while the valley bias position and current are almost stationary, behavior that is qualitatively different to that for the two in-plane orientations, in which the peak current remains constant with field, while the valley bias and current both increase. The shifts in bias and current for the [001] field orientation are probably related to the nonparabolicity of the X band where the Landau-level separations associated with $X_t(2)$ are slightly different from those associated with $X_t(1)$.

In all cases, we assume that the quasi-Fermi level in the GaAs emitter layer remains pinned to the lowest emitter $X_t(1)$ state. Since the cyclotron energy in this layer increases much more rapidly with field than the energy of the lowest emitter $X_t(1)$ state, the effect for all field orientations of increasing the field from zero to 15 T is similar to a pressure increase of about 1 kbar. Such a pressure change on its own would correspond to a small bias increase,[8] but this should be compensated for almost exactly by a corresponding increase in cyclotron energy in the GaAs collector contact, which raises the energy of the collector quasi-Fermi level. Shifts in the phonon-assisted resonances $X_t(1) \rightarrow X_t(1) + \mathrm{TO_{GaAs}}$ and $X_t(1) \rightarrow X_t(1) + \mathrm{TO_{AlAs}}$ with parallel magnetic field (the two features in the 100–200-mV bias regions in Fig. 1, discussed in detail in Ref. 8) show that cyclotron energy changes in the contacts change the bias by less than 3 meV. While this change is small, it may be enough to affect slightly the accuracy of the Schrödinger-Poisson model used below to fit the observed bias shifts for $X_t(1) \rightarrow X_t(2)$, assuming that they are all due to the field induced wave-vector change between $X_t(1)$ and $X_t(2)$. The results of such fits should therefore only be taken as indicative and not definitive. The effect on fitting the Landau-level features reported in Ref. 15, however, is negligible, due to the much larger field-induced shifts of these features.

The Schrödinger-Poisson model has been shown to be reliable at the bias of the $X_t(1) \rightarrow X_t(2)$ resonance, and indeed the same field dependences are measured at pressures less than P_t, for which it has been most stringently tested.[8] With Eq. 2, the model gives a value for the effective mass associated with the $\mathbf{B}\|[100]$ field dependence, $m_y^* = (0.93 \pm 0.11) m_0$. This is based on results at four field values in both bias directions for one sample with $l_w = 70$ Å, and one sample with $l_w = 60$ Å, and takes into account the $\pm 5°$ orientation error. It is consistent with the heavy effective mass of the X minima, for which the current evaluation is $m_{X,L}^* = (1.1 \pm 0.2) m_0$,[18] and therefore supports the postulation that the effect is dominated by the X_y minima. However, it should be noted that for $\mathbf{B}\|[110]$, a mass of $m_y^* = (0.81 \pm 0.14) m_0$ is deduced from a similar analysis for two samples with $l_w = 70$ Å and one with $l_w = 60$ Å. This is significantly larger than the theoretical value, which is derived on the basis of a perfectly ellipsoidal Fermi surface as

$$m_{[110]}^* = \frac{2 m_{X,L}^* m_{X,T}^*}{m_{X,L}^* + m_{X,T}^*} \approx (0.4 \pm 0.1) m_0 \qquad (4)$$

[also using the value of the light principal effective mass,[8,9,18] $m_{X,T}^* = (0.24 \pm 0.05) m_0$]. The reason for the discrepancy for $\mathbf{B}\|[110]$ is not clear, but may perhaps be related to the camel's back nature of the X-band edge which has not been taken into account in the preceding analysis.

IV. SUMMARY

We have carried out magnetotunneling experiments that probe the in-plane dispersions of the transverse X minima in AlAs. The results demonstrate the influence of the Lorenz force on the tunneling electrons, with a strong splitting of the zero-bias $X_t(1) \rightarrow X_t(1)$ conductance peak, and an upward shift in the bias position of the $X_t(1) \rightarrow X_t(2)$ resonance. Anisotropy observed between the $\mathbf{B}\|[100]$ and $\mathbf{B}\|[110]$ crystal orientations indicates that electrons occupying the X_y minima dominate the tunneling current when $\mathbf{B}\|[100]$, and quantitative analysis of the bias shifts using a Schrödinger-Poisson model provides limited support for this conclusion.

Note added in proof. Our most recent detailed measurements[19] of the voltage bias as a function of the angle of the in-plane magnetic field have shown that the disper-

sions in the [110] and $[\bar{1}10]$ directions are changed from the bulk dispersion and are no longer equivalent, and that there is only a single dispersion in the ⟨100⟩ directions. These results are interpreted in terms of X_x-X_y mixing. In the present work, this explains the absence of a second feature for $\mathbf{B}\|[100]$ and the anomalous value obtained for the effective mass in the [110] direction.

ACKNOWLEDGMENTS

This work was funded by the Engineering and Physical Sciences Research Council (EPSRC), and J. M. S. acknowledges additional support from the General Electric Company (GEC). We also thank Dr. M. E. Eremets for his work in the design and construction of the pressure cell.

*Present address: Research Department (0500), Electronics and Telecommunications Research Institute (ETRI), 161 Kajong-dong-Gu, Taejon 305-350, South Korea.

[1] I. Hase, H. Kawai, K. Kaneko, and N. Watanabe, J. Appl. Phys. **59**, 3792 (1986).

[2] E. E. Mendez, E. Calleja, C. E. T. Gonçalves da Silva, L. L. Chang, and W. I. Wang, Phys. Rev. B **33**, 7368 (1986).

[3] P. M. Solomon, S. L. Wright, and C. Lanza, Superlattices Microstruct. **2**, 521 (1986).

[4] A. R. Bonnefoi, T. C. McGill, R. D. Burnham, and G. B. Anderson, Appl. Phys. Lett. **50**, 344 (1987).

[5] D. G. Austing, P. C. Klipstein, J. S. Roberts, and G. Hill, Solid State Commun. **75**, 697 (1990).

[6] E. E. Mendez and L. L. Chang, Surf. Sci. **229**, 173 (1990).

[7] D. G. Austing, P. C. Klipstein, A. W. Higgs, H. J. Hutchinson, G. W. Smith, J. S. Roberts, and G. Hill, Phys. Rev. B **47**, 1419 (1993).

[8] J. M. Smith, P. C. Klipstein, R. Grey, and G. Hill, Phys. Rev. B **57**, 1740 (1998).

[9] J. J. Finley, R. J. Teissier, M. S. Skolnick, J. W. Cockburn, R. Grey, G. Hill, and M. A. Pate, Phys. Rev. B **54**, R5 251 (1996).

[10] D. G. Austing, P. C. Klipstein, J. S. Roberts, C. B. Button, and G. Hill, Phys. Rev. B **48**, 11 905 (1993).

[11] J. Smoliner, W. Demmerle, G. Berthold, E. Gornik, G. Weimann, and W. Schlapp, Phys. Rev. Lett. **63**, 2116 (1989).

[12] M. L. Leadbeater, E. S. Alves, L. Eaves, M. Henini, O. H. Hughes, A. Celeste, J. C. Portal, G. Hill, and M. A. Pate, J. Phys.: Condens. Matter **1**, 4865 (1989).

[13] Ulf Gennser, V. P. Kesan, D. A. Syphers, T. P. Smith, S. S. Iyer, and E. S. Yang, Phys. Rev. Lett. **67**, 3828 (1991).

[14] A. P. Heberle, M. Oestreich, S. Haacke, W. W. Rühle, J. C. Maan, and K. Köhler, Phys. Rev. Lett. **72**, 1522 (1994).

[15] J. M. Smith, P. C. Klipstein, R. Grey, and G. Hill, Phys. Rev. B **57**, 1746 (1998).

[16] J. M. Heisz and E. Zaremba, Semicond. Sci. Technol. **8**, 575 (1993).

[17] Frank Stern and W. E. Howard, Phys. Rev. **163**, 816 (1967).

[18] S. Adachi, *GaAs and Related Materials; Bulk Semiconducting and Superlattice Properties* (World Scientific, Singapore, 1994).

[19] H. Im and P. C. Klipstein (unpublished).